Synthesis of Pt Nanopetals on Highly Ordered Silicon Nanocones for Enhanced Methanol Electrooxidation Activity

Jitendra N. Tiwari,*,† Rajanish N. Tiwari,† and Kun-Lin Lin‡

Department of Materials Science and Engineering, National Chiao Tung University, 1001 Ta Hsueh Road, Hsinchu, Taiwan, 30050, R.O.C., and Department of Mechanical Engineering, National Taiwan University of Science and Technology, Taipei 0660, Taiwan, R.O.C.

ABSTRACT Platinum (Pt) nanopetals were electrodeposited on highly ordered silicon nanocones (SiNCs) and explored as the electrocatalyst for methanol oxidation reaction (MOR) for direct methanol fuel cells applications. Highly ordered SiNCs array fabricated using the porous anodic aluminum oxide as the template had a high surface area. Well-dispersed Pt nanopetals possessing high electrocatalytic surface area was synthesized by pulse-electrodeposition on the SiNCs. Pt nanopetals loaded on highly ordered SiNC support exhibited very good catalytic activity for MOR and a high tolerance against CO poisoning, as compared to Pt nanoflowers/flat Si, Pt nanoparticles/flat Si, and many previously reported works. The abundance of a large surface area for facile transport of methanol, SiO_2 sites in the vicinity of the SiNCs, as well as less contact area between the Pt nanopetals catalyst and SiNCs are suggested to be the major factors enhancing the electrocatalytic performance of the Pt nanopetal/SiNC electrode. Moreover, we believe this new nanostructure (Pt nanopetals/SiNCs) will enable many new advances in nanotechnology.

KEYWORDS: 3D/3D nanoarchitecture • Pt nanopetals • methanol oxidation • fuel cells

Since the discovery of potential applications of one-dimensional (1D), two-dimensional (2D) and three-dimensional (3D) platinum (Pt) nanostructures, research and development on nanostructures have been intensively conducted worldwide (1−9). The 1D, 2D, and 3D Pt nanostructure materials have been synthesized from atoms and molecules of themselves, namely, self-assembly, to become nanoscaled particles, nanotubes, nanowires, nanoplatelets, nanoflowers, etc. (1−9). They possess exceptional properties different from bulk materials such as electrical, optical, magnetic, physical, or chemical. Therefore, the 1D, 2D, and 3D Pt nanostructures have high potential applications (1−9). Among these nanostructures, well-controlled 3D nanostructures with high yield are particularly interesting because of their high catalytic activity in catalytic reactions. In the past few years, several chemical methods have been developed for the synthesis of 3D Pt nanostructures, but most of the chemical methods are either tedious or difficult to control making exceedingly challenging for the researchers to the synthesis of 3D Pt nanostructures.

In addition, the cost of Pt catalysts is too high and the synthesized 3D nanostructures on flat support display catalytic activity only in spatial orientation. Therefore, researchers need to devise new architecture to maximize net catalytic active surface area of the Pt nanostructures for fuel cell applications to reduce the costs of electrochemical devices. Thus, we can reduce the cost of direct methanol fuel cell (DMFCs) to make them viable in many new commercial applications.

Toward this aim, we report here for the first time the fabrication of nanopetals on the highly ordered silicon nanocones (SiNCs) and studied the electrocatalytic performance of the fabricated nanopetals/SiNCs electrode in methanol oxidation for DMFC applications. The Pt nanopetals catalyst were deposited on the SiNCs by potentiostatic bipolar pulse electrodeposition. Because the Pt nanopetals was synthesized directly on the SiNCs of a low resistivity (0.002 Ω cm), which acted as the current collector, the SiNCs support was very suitable for use as the Pt electrocatalytic electrode in respect of electrical conductivity.

As shown in Scheme 1, the presence of large surface area for facile transport of fresh methanol, SiO_2 sites in the vicinity of the SiNCs, as well as less contact area between the Pt nanopetals catalysts and SiNCs array, can greatly enhance the electrocatalytic activity of the Pt nanopetals/SiNCs electrode toward oxidation of methanol and CO adspecies. Moreover, the electrocatalytical study of the Pt nanopetals/SiNCs indicates the potential application for electrodes in DMFCs.

EXPERIMENTAL METHODS

Fabrication Procedure for the SiNCs. The fabrication procedure of the highly ordered SiNCs is schematically illustrated in Figure 1. A p-type 4 in. silicon wafer of low resistivity (0.002 Ω cm) was used as the substrate for the fabrication of SiNCs. A TiN thin film ∼30 nm thick was first sputter-deposited on the silicon surface, followed by thermal evaporation of an aluminum thin film ∼1 μm thick. The TiN layer was used as the adhesion layer between the silicon substrate and the Al thin

* Corresponding author. E-mail: jnt_tiw123@yahoo.co.in.
Received for review March 23, 2010 and accepted July 9, 2010
† National Chiao Tung University.
‡ National Taiwan University of Science and Technology.
DOI: 10.1021/am100256g

Scheme 1. Schematic Illustration of (a) Pt Nanoparticle on Flat Si Substrate, (b) Pt Nanoflower on Flat Si Substrate, and (c) Pt Nanopetal on SiNC Substrate[a]

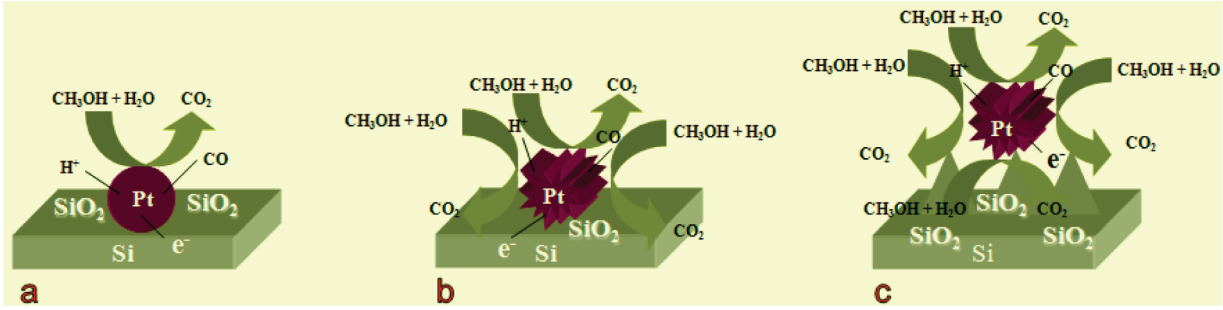

[a] Among a, b, c nanostructures, c shows maximum utilization of Pt catalyst. Thus, the electrocatalytic activity can be improved in case c. In addition, schemes a−c show the bifunctional mechanism of CO oxidation. The adsorbed O_2-containing species on the surface of SiO_2 can assists the oxidation of CO-like adspecies adsorbed on the active Pt sites.

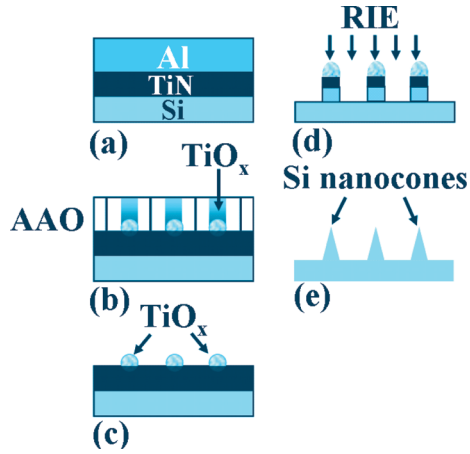

FIGURE 1. Fabrication processes of ordered SiNCs: (a) deposition of TiN and Al thin films on the silicon wafer by sputter deposition and thermal evaporation, respectively, (b) formation of the porous anodic aluminum oxide (AAO) template and TiOx nanodots in the AAO pore channels, (c) elimination of AAO by wet etch, (d) reactive ion etch of the remaining TiN, (e) reactive ion etch of the silicon substarte, and forming the SiNCs.

film, and would be later used for preparation of the nanodot mask for fabrication of the SiNCs. The as-deposited Al/TiN film stack was then oxidized by electrochemical anodization, which was performed in a 0.3 M oxalic acid ($H_2C_2O_4$) aqueous solution at 25 °C under a constant polarization voltage of 40 V for 20 min. Anodic oxidation of the Al thin film under the anodization conditions produced hexagonally arranged anodic aluminum oxide (AAO) nanopore channels. As the anodization reaction approached the interface between the Al and TiN thin films, local anodization of the underlying TiN layer occurred, forming the TiO_2 nanodot mask on the TiN layer. The AAO was then removed by the aqueous solution of 6 wt % H_3PO_4 and 1.5 wt % CrO_3 at 70 °C for 40 min, followed by etching the TiN-capped silicon substrate by inductively coupled-plasma reactive-ion-etch (RIE) for 40 s. with the remaining TiO_2 nanodots as the mask, using a gas mixture of BCl_3 and Cl_2 as the plasma source. The RIE process was performed under the following working conditions: plasma power 400 W, substrate bias power 120 W, working pressure 10 mTorr with a flow rate of 35 sccm for the plasma gas source.

Synthesis of Pt Nanopetals on the SiNCs. The Pt nanopetals were electrodeposited on SiNC arrays in the aqueous solution of 1 M H_2PtCl_6−1 M H_2SO_4 at room temperature by the potentiostatic pulse plating in a three-electrode cell system. A saturated calomel reference electrode (SCE) was used as the reference electrode. The highly ordered SiNCs array was the working electrode and the counter electrode was a thin platinum wire. The preparation conditions for Pt nanopetals have been optimized. The time durations for the upper potential pulse (0.6 V) and the lower potential pulse (−0.2 V) were 8 and 1 ms, respectively. For synthesis of nanoflowers, the time durations for the upper potential pulse (0.5 V) and the lower potential pulse (−0.2 V) were 7 and 1 ms, respectively. After all samples prepared, the samples was washed with deionized water to remove contamination from the sample surface, and dried under ambient conditions. For comparison, we also deposited the Pt nanoparticles on the flat Si substrates by using a bipolar pulse electrodeposition. The mass loading of the Pt catalyst on the electrodes were determined by measuring the difference in the mass of the electrodes before and after Pt deposition, using a microbalance (Sartorious, PB-SAH).

Physicochemical Characterization. The surface morphology of the samples was examined with a scanning electron microscopy (SEM, JEOL JSM-6700F). The X-ray photoelectron spectroscopy (XPS, Thermo VG 350) analysis was carried out with the Mg Kα radiation (1253.6 eV) to study the chemical composition of the Pt nanopetals/SiNCs electrode. Transmission electron micrographs were obtained by a JEOL JEM-3000F transmission electron microscope (TEM) operated at 200 kV. The TEM specimen was prepared by mechanically scratching the Pt nanopetals using dissecting forceps in the presence of a small drop of ethanol. The scratched specimen was put onto a holey-copper grid and dried in air at room temperature.

Electrochemical Studies. The electrochemical studies were carried out on a Jihan 5000 electrochemical workstation. A traditional three-electrode cell involved a Pt wire as counter electrode, a SCE as reference, and samples as working electrode. All the solutions were prepared with high-purity deionized water from a Millipore Milli-Q purification system (resistivity ~18 MΩ cm). The Pt nanopetals/SiNC electrode was rinsed thoroughly with deionized water to remove residual chlorine ions after Pt electrodeposition, and allowed to dry before use in the measurement cell. Methanol electrocatalytic oxidation measurements were carried out in a mixture of 1 M H_2SO_4 (Aldrich, 99%) and 1 M methanol (Sigma-Aldrich, > 99%) at the scan rate of 25 mV s^{-1}. All the electrochemical experiments were conducted at 25 °C.

RESULTS AND DISCUSSION

The SEM is an essential tool for the precise characterization of nanostructured materials. Hence, we used SEM to analyze the surface images of the all specimens. Figure 2 contains several SEM images of nanostructured materials. Figure 2A shows typical SEM image of Pt nanoparticles/flat Si. The Pt nanoparticles have a diameter of about ~500 nm, as shown in Figure 2A. Figure 2B shows typical SEM image

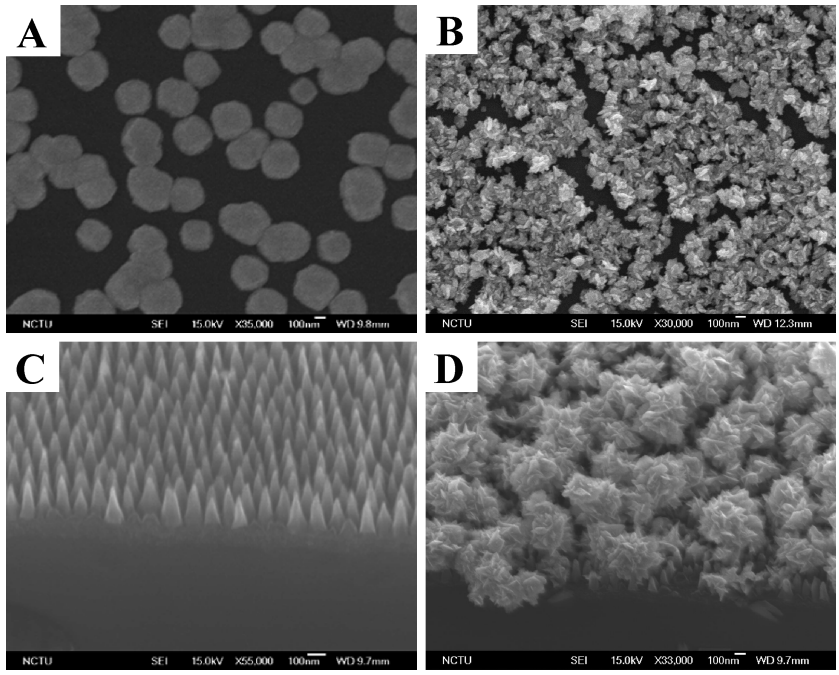

FIGURE 2. SEM images of (A) electrodeposited Pt nanoparticles/flat Si, (B) Pt nanoflowers/flat Si, (C) highly ordered SiNCs, and (D) electrodeposited of Pt nanopetals on SiNCs.

of Pt nanoflowers/flat Si. The Pt nanoflowers have a diameter of about ~300 nm and seem to agglomerate more easily with each other. Figure 2C shows an SEM image of the SiNCs prepared by using anodic aluminum oxide template method. From Figure 2C, it is clear that we successfully fabricated the highly ordered SiNCs. And the individual nanocone had a size of about ~100 nm. Figure 2D shows a typical SEM image of the Pt nanopetals/SiNCs, which was synthesized by potentiostatic-pulse method. It is clearly seen that Pt nanopetals are homogeneously dispersed on the SiNCs, and their diameter ranges from ~500 to ~800 nm. In addition, the side face of the nanopetal is not smooth, and several sharp edges appear. The detailed morphology of the Pt nanopetals has been further examined by TEM and HRTEM images, as shown later.

X-ray photoelectron spectroscopy (XPS) is another powerful tool to investigate the chemical compositions of all samples. Thus, XPS was used to characterize the surface properties of the all specimens. Figure 3 contains the XPS spectra of the three electrodes. The XPS results clearly show that the presence of the Pt catalysts on the three samples, as shown in Figure 3. And no XPS signal associated with Si(2s) and Si(2p) from the Pt nanopetals/SiNCs were observed, suggesting that fabricated SiNC arrays were covered with a synthesized Pt nanopetals.

To gain further insight into the Pt nanopetals/SiNCs electrode, we analyzed the Pt nanopetal by bright-field transmission electron microscope (TEM), bright-field high-resolution TEM (HRTEM), fast Fourier transform (FFT), and selected area electron diffraction (SAD) pattern, respectively. Figure 4A shows the TEM image of a Pt nanopetal. The inset to Figure 4A displays the corresponding HRTEM image of the tip of a nanopetal marked in Figure 4A. The continuous fringe pattern and the inset FFT pattern on the upper right

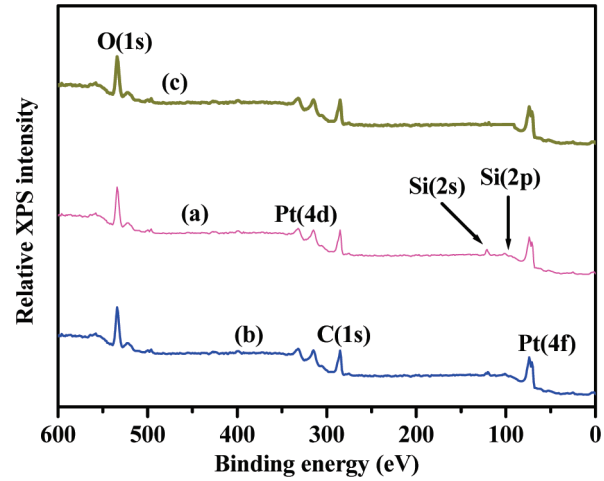

FIGURE 3. XPS spectra of (a) electrodeposited Pt nanoparticle/flat Si electrode, (b) Pt nanoflower/flat Si electrode, and (c) electrodeposited Pt nanopetal/SiNC electrode. The XPS results clearly show the presence of Pt catalysts.

corner of HRTEM image and indicates that the single-crystalline property of the nanopetal. As shown in the inset to Figure 4A, the Pt nanopetal has grown along the ⟨111⟩ direction, and the distance between the {111} planes is 0.23 nm, which is in agreement with that found for bulk Pt crystals. The Figure 4B shows the corresponding SAD patterns, which can be indexed to face-centered cubic (FCC) structure. It is noteworthy that several distinct diffraction spots instead of continuous rings appear in the SAD pattern, which indicates that the Pt nanopetals possess a good crystallinity.

The hydrogen adsorption and desorption is a powerful technique to determine the electrochemical active surface area (ESA) of a Pt electrode. By means of hydrogen adsorption/desorption methods and with cyclic voltammetry (CV),

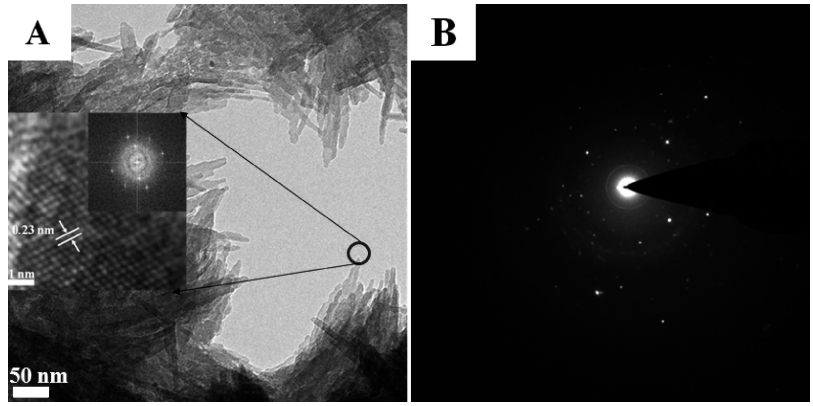

FIGURE 4. (A) Bright-field TEM image of the Pt nanopetals (inset, HRTEM image of the nanopetal marked in (A), and the inset of the HRTEM image is the corresponding FFT image); and (B) the selected area electron diffraction (SAD) pattern.

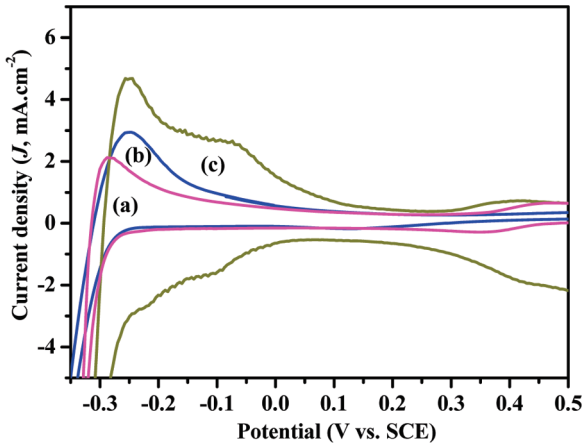

FIGURE 5. Hydrogen electrosorption cyclic voltammetry curves for (a) electrodeposited Pt nanoparticles/flat Si, (b) Pt nanoflowers/flat Si, and (c) electrodeposited Pt nanopetals/SiNC electrodes in an N_2 saturated 1 M H_2SO_4 solution. The scan rate is 25 mV s^{-1}.

the ESA of Pt can be measured. We calculated the ESA of each sample using the following equation (10, 11)

$$\mathrm{ESA} = Q_H/(0.21W) \qquad (1)$$

where Q_H reveals the number of Pt sites available for hydrogen adsorption/desorption (mC cm^{-2}); the correlation constant of 0.21 (mC cm^{-2}) represents the charge required to oxidize a monolayer of hydrogen on a smooth Pt surface. W represents the Pt loading (mg cm^{-2}) in the electrode. For comparison, a Pt nanoflower/flat Si electrode, and Pt nanoparticle/flat Si electrode were also investigated. All cyclic voltammetry (CV) curves in this study refer to the features in the second cycle, where a steady-state response was obtained.

The values of Q_H measured under the electro-adsorption curves (Figure 5) for hydrogen on the Pt nanopetal/SiNC, Pt nanoflower/flat Si, and Pt nanoparticle/flat Si electrodes were ~64.5, ~48.7, and ~25.6 mC cm^{-2}, respectively; microbalance analysis revealed that the Pt loadings were ~0.26, ~0.39, and ~0.63 mg cm^{-2}, respectively. Putting these values into eq 1, we calculated the ESA values of the Pt nanopetal/SiNC, Pt nanoflower/flat Si, and Pt nanoparticle/flat Si electrodes to be 118.1, 59.4, and 19.4 m^2 g^{-1}, respectively. The ESA value of the Pt nanopetals/SiNCs electrode is larger than that of Pt nanoflowers/flat Si and Pt nanoparticles/flat Si electrodes and many other previously reported electrodes (12−14) (see Table 1). The high ESA of the Pt nanopetals/SiNCs electrode is attributed to 3D/3D nanoarchitecture. The resistance to the flow of liquid and gas through the 3D/3D structure is due to the maximum utilization of precious Pt catalyst and less contact area between the Pt nanopetal catalyst as well as the SiNC array.

Table 1. ESA Data of the Different Electrodes at Room Temperature

electrode	hydrogen electrosorption CV (m^2g^{-1})
Pt nanopetals/SiNCs	118.1[a]
Pt nanoflowers/flat Si	59.4[a]
Pt nanoparticles/flat Si	19.4[a]
Pt nanonetwork(12)	77[b]
Pt nanosponge(12)	70.4[b]
Pt nanodendrite(12)	41.4[b]
Pt nanosheet(13)	104.8[c]
Pt/CNx(14)	104[d]
Pt/PPy(14)	117[d]
Pt/XC-72(14)	84[d]

[a] Scan rate 25 mVS^{-1}, electrolyte 1 M H_2SO_4. [b] Scan rate 50 mVS^{-1}, electrolyte 1 M H_2SO_4. [c] Scan rate 50 mVS^{-1}, electrolyte 0.1 M H_2SO_4. [d] Scan rate 50 mVS^{-1}, electrolyte 1 M H_2SO_4.

Carbon monoxide (CO) stripping CV was used further to calculate the ESA of the electrdoes. The CO-stripping CV experiments were performed in a CO saturated 1 M H_2SO_4 aqueous solution using a Pt wire as the counter electrode and SCE as the reference electrode. The scan rate for CO stripping was 25 mV s^{-1}. The ESA of the electrode was calculated by integrating the electrooxidation peak of linearly adsorbed CO molecules, assuming an electrooxidation charge of 420 μC cm^{-2} for a monolayer of CO adspecies on a polycrystalline Pt surface (15). The CO-stripping CV curves for the Pt nanoparticles/flat Si, Pt nanoflowers/flat Si, and Pt nanopetales/SiNCs electrodes are shown in Figure 6a−c. The ESA values for Pt nanoparticle/flat Si, Pt nanoflower/flat Si, and Pt nanopetal/SiNC electrodes were 17.6, 52.7, and 106.8 m^2 g^{-1}, respectively. In addition, as shown in Figure 6 a−c, the peak current intensity of CO electrooxidation on

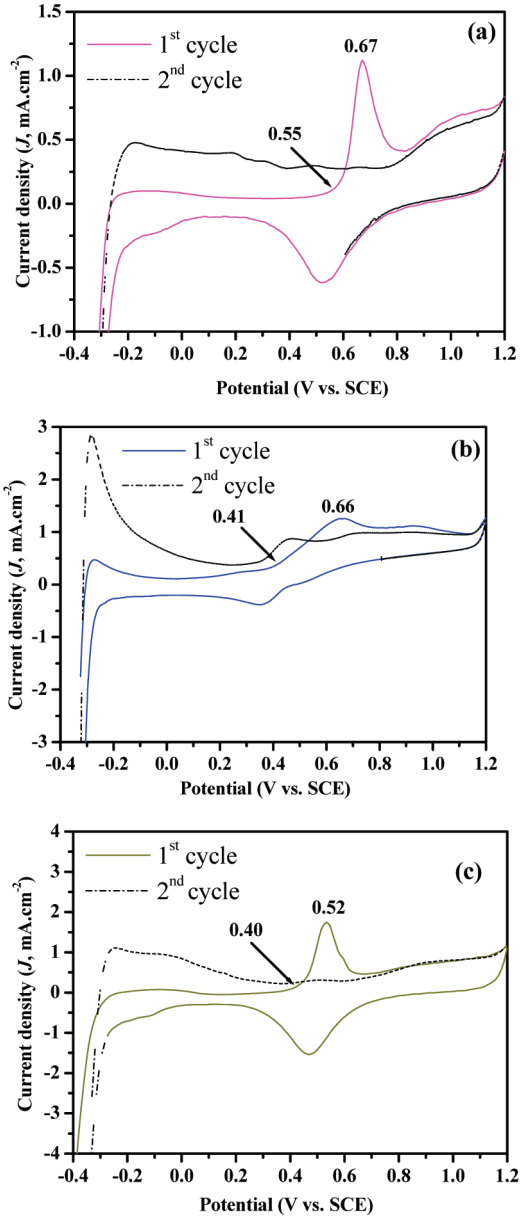

FIGURE 6. CO stripping cyclic voltammetry curves for (a) electrodeposited Pt nanoparticles/flat Si, (b) Pt nanoflowers/flat Si, and (c) electrodeposited of Pt nanopetals/SiNCs electrodes in an CO saturated 1 M H_2SO_4 solution. The scan rate is 25 mV s^{-1}.

Pt nanopetals/SiNCs is much larger than Pt nanoparticles/flat Si and Pt nanoflowers/flat Si, further showing that the Pt nanopetals/SiNCs have very high ESA. The above results indicate that the Pt nanopetal/SiNC electrode possesses a much higher ESA compared to the Pt nanoparticle/flat Si and Pt nanoflower/flat Si electrodes. This is consistent with the results obtained in Figure 5.

However, one of the important factors in DMFCs is efficient removal of the CO adspecies from the catalyst surface. The CO-stripping CV curves also provide the information about the CO tolerance over the Pt nanoparticles/flat Si, Pt nanoflowers/flat Si, and Pt nanopetals/SiNCs electrodes. As shown in Figure 6a–c during the first forward cycle, when the potential was scanned from −0.4 to 0.0 V, the CV curve was suppressed, indicating that hydrogen adsorption is completely suppressed because the available

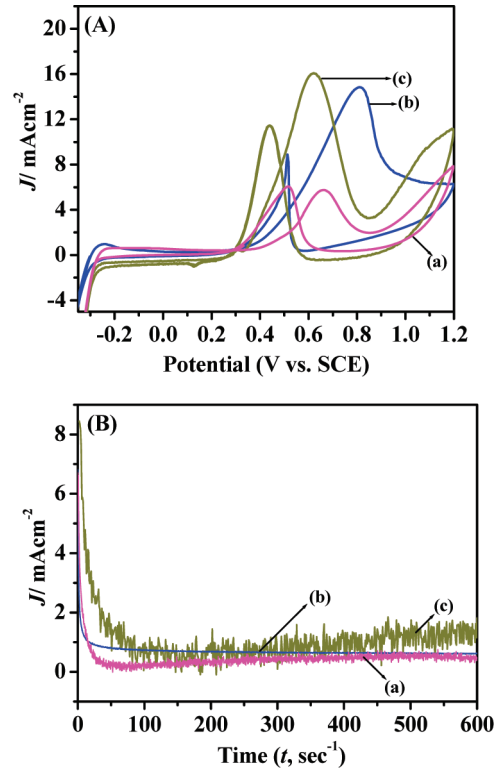

FIGURE 7. (A) Cyclic voltammetry plots (scan rate: 25 mVs^{-1}) and (B) current–time curves (fixed potential: 0.4 V) of (a) electrodeposited Pt nanoparticle/flat Si, (b) Pt nanoflower/flat Si, and (c) electrodeposited of Pt nanopetal/SiNC electrodes in N_2-saturated 1 M H_2SO_4–1 M CH_3OH. The current density *j* was normalized in reference to the electrochemical active surface area of Pt.

active Pt sites were completely covered by adsorbed CO. The onset potential of CO electrooxidation on the Pt nanoparticle/flat Si, Pt nanoflower/flat Si, and Pt nanopetal/SiNC electrodes was about ~0.55, ~0.41, and ~0.39 V, respectively. This result demonstrates that the Pt nanopetals/SiNCs electrode can oxidize the adsorbed CO-like adspecies more efficiently than Pt nanoparticles/flat Si, and Pt nanoflowers/flat Si at the lower electrode potentials. In addition, the CO electrooxidation current peaks of the Pt nanoparticle/flat Si, Pt nanoflower/flat Si, and Pt nanopetal/SiNC electrodes were centered at ~0.67, ~0.66, and ~0.52 V, respectively. Further, Pt nanopetals/SiNCs electrode shows the center current peak is lower. The lower onset potential and lower center current peak of the CO electrooxidation, as well as the higher ESA clearly demonstrates that the Pt nanopetal/SiNC electrode could effectively improve the electroactivity of the Pt catalyst toward methanol oxidation. The improvement on electrooxidation activity of CO adspecies on the Pt nanopetal/SiNC electrode may be ascribed to the SiO_2 sites at the Pt nanopetals-SiNCs boundaries facilitate the nucleation of oxygen-containing species (OH_{ads}), thus oxidizing the adsorbed CO-like adspecies at a lower electrode potential.

We further studied the electrocatalytic activity of the Pt nanoparticle/flat Si, Pt nanoflower/flat Si, and Pt nanopetal/SiNC electrodes toward methanol oxidation reaction. Figure 7A shows their CV curves in a solution of 1 M H_2SO_4–1 M CH_3OH solution at a scan rate of 25 mV s^{-1}. The current density has been normalized to ESA Pt surface area so that

Table 2. CV Data of the Different Electrodes for Methanol Oxidation at Room Temperature

electrode	onset potential (V)	forward peak potential (V)	current density (mA/cm^2)
Pt nanopetals/SiNCs	0.26	0.61[a]	19.02[a]
Pt nanoflowers/flat Si	0.35	0.81[a]	8.77[a]
Pt nanoparticles/flat Si	0.45	0.66[a]	1.12[a]
Pt/CNx(14)	0.4	0.66[b]	7[b]
Pt/PPy(14)	0.4	0.66[b]	14.1[b]
Pt/GMC900(16)	0.43	0.65[c]	0.66[c]
Pt/GMC1000(16)	0.39	0.66[c]	0.98[c]
Pt/C-1(17)	0.41	0.65[c]	1.39[c]
Pt/C-2(17)	0.45	0.65[c]	1.25[c]

[a] Scan rate 25 mVS^{-1}, electrolyte 1 M methanol -1 M H_2SO_4. [b] Scan rate 50 mVS^{-1}, electrolyte 1 M methanol -1 M H_2SO_4. [c] Scan rate 20 mVS^{-1}, electrolyte 1 M methanol -0.5 M H_2SO_4.

the current density (*j*) can be directly used to compare the catalytic activity of different electrodes. As shown in Figure 7A, the onset potential for methanol oxidation of the Pt nanoparticle/flat Si, Pt nanoflower/flat Si, and Pt nanopetal/SiNC electrodes were ∼0.43, ∼0.39, and ∼0.35 V, respectively. The negative onset potential shifting indicated that Pt nanopetals/SiNCs can effectively reduce overpotentials in the methanol electrooxidation reaction. It should be noted that the current density of Pt nanopetals/SiNCs is also higher than those of Pt nanoparticles/flat Si, Pt nanoflowers/flat Si. The higher methanol oxidation peak current densities observed from CVs suggest that Pt nanopetal/SiNC electrode exhibited better electrooxidation activity. Therefore, this implies that the Pt nanopetals/SiNCs for the methanol electrooxidation has excellent electrocatalytic activity compared with the Pt nanoparticles/flat Si, Pt nanoflowers/flat Si. In addition, it should be noted that the current density (without normalized to ESA Pt surface area) of Pt nanopetals/SiNCs (Figure not shown) is also higher than those of Pt nanoparticles/flat Si, Pt nanoflowers/flat Si, and many previously reported (14, 16, 17) (Table 2).

Finally, we performed chronoamperometry measurements to evaluate the catalytic activity and long-term stability of our three electrodes in a N_2-saturated aqueous solution of 1 M CH_3OH−1 M H_2SO_4 at 25 °C at a constant potential of ∼0.4 V (vs SCE). The chronoamperometry curves of methanol electrooxidation on Pt nanopetals/SiNCs, Pt nanoflowers/flat Si, and Pt nanoparticles/flat Si electrodes are shown in Figure 7B. The current density has been normalized to ESA Pt surface area so that the current density (*j*) can be directly used to compare the catalytic activity of different electrodes. As shown in Figure 7B, all three electrodes exhibited current decays during the initial stage because of the formation of intermediate species (e.g., CO and CHO adspecies), similar to the observations previously reported (18). The rapid fall in the initial current density of the three electrodes followed the order Pt nanopetals/SiNCs > Pt nanoflowers/flat Si > Pt nanoparticles/flat Si.

In addition, the higher onset current densities and increase in electrooxidation current density is indicative of better CO-resistance. The onset current densities at Pt nanopetal/SiNC, Pt nanoflower/flat Si, and Pt nanoparticle/flat Si electrodes are ca. 8.4, 6.7, and 6.4, respectively. It is also observed that Pt nanopetals/SiNCs exhibited higher mass current density than the Pt nanoflowers/flat Si, and Pt nanoparticles/flat Si during the entire testing time. The current density at Pt nanopetals/SiNCs electrode at 600 s is almost 2.4 and 2.85 times larger than that at Pt nanoflower/flat Si and Pt nanoparticle/flat Si electrodes, respectively. As shown in Figure 7B, the Pt nanopetals/SiNCs electrode shows the current density gradually increases with the time. We believe that this behavior is related mainly because the surface area of the Pt nanopetal assemblies was large, which in turn enhanced the diffusion of fresh methanol into the SiNCs electrode surface. These results further demonstrate the improved catalytic activity and stability of Pt nanopetal/SiNC electrode in comparison to Pt nanoflower/flat Si and Pt nanoparticle/flat Si electrodes. Thus, all the above data reveal that the as-prepared Pt nanopetal/SiNC electrode shows high electrocatalytic activity toward MOR.

The Pt nanopetals/SiNCs electrode exhibits a good stability, and high electrocatalytic activity toward oxidation of methanol and CO adspecies because of the following factors:

(1) The synthesized 3D/3D nanostructured may give high ESA. The high ESA of 3D/3D nanostructure is attributed to larger open volume, which facilitates fresh methanol to diffuse/be included more easily between Pt catalysts through SiNCs. Hence, higher electrocatalytic activity can be achieved by 3D/3D nanostructures.

(2) The 3D/3D nanostructure electrode having large active catalytic surface area could provide high population of the active sites for catalytic reactions, so as to enhance the electrocatalytic activity (as shown in Scheme 1).

(3) It has been reported that the function of SiO_2 is similar to Ru as in Pt−Ru/C catalysts (19). Pt acts as the main catalyst for the dehydrogenation of methanol during the oxidation reaction, and oxygen-containing species (OH_{ads}) can be provided by SiO_2. These oxygen-containing species react with CO-like species on the Pt surface to release the active sites for further methanol oxidation.

This implies that the Pt nanopetals/SiNCs could represent a promising electrode for DMFCs. The Pt nanopetal/SiNC electrode can be monolithically integrated with other major components of DMFC such as gas diffusion layer, flow field, membrane, and current collector. Fuel reservoirs were also integrated into the system so that liquid fuel (e.g., methanol) can be used (20).

CONCLUSIONS

In summary, the Pt nanopetals catalysts have been successfully synthesized by potentiostatic pulse plating on the highly ordered silicon nanocones (SiNCs) array, and electrochemical measurements confirm that this Pt nanopetals on the SiNCs array has a better electro-activity toward methanol oxidation than the Pt nanoparticles/flat Si and the Pt nanoflowers/flat Si electrodes. The excellent electrocatalytic performance can be ascribed to the presence of large surface area for facile transport of methanol, SiO_2 sites through bottom side of the SiNCs, as well as less contact area

between the Pt nanopetals and SiNCs array, which significantly enhanced the oxidation of methanol and CO tolerance and thus improved the electrocatalytic activity of the Pt nanopetal/SiNCs array. Moreover, we believe that the applications of the new nanostructures, such as Pt nanopetal/SiNC are not only for fuel cell development, but also for sensors, capacitors, surface enhanced Raman scattering (SERS), etc.

Acknowledgment. The authors thank Prof. Fu-Ming Pan for availing us all the necessary lab facilities, chemicals, and reagents.

REFERENCES AND NOTES

(1) Lee, E. P.; Peng, Z.; Chen, W.; Chen, S.; Yang, H.; Xia, Y. *ACS Nano* **2008**, *2*, 2167–2173.
(2) Liu, J.; Cao, G.; Yang, Z.; Wang, D.; Dubois, D.; Zhou, X.; Graff, G. L.; Pederson, L. R.; Zhang, J.-G. *ChemSusChem* **2008**, *1*, 676–697.
(3) Guo, Y.-G.; Hu, J.-S.; Wan, L.-J. *Adv. Mater.* **2008**, *20*, 2878–2887.
(4) Rolison, D. R.; Long, J. W.; Lytle, J. C.; Fischer, A. E.; Rhodes, C. P.; McEvoy, T. M.; Bourga, M. E.; Lubersa, A. M. *Chem. Soc. Rev.* **2009**, *38*, 226.
(5) Cui, G.; Zhi, L.; Thomas, A.; Kolb, U.; Lieberwirth, I.; Mullen, K. *Angew. Chem., Int. Ed.* **2007**, *46*, 3464–3467.
(6) Chen, J.; Lim, B.; Lee, E. P.; Xia, Y. *Nano Today* **2009**, *4*, 81–95.
(7) Tiwari, J. N.; Pan, F.-M.; Tiwari, R. N.; Nandi, S. K. *Chem. Commun.* **2008**, *48*, 6516–6518.
(8) Tiwari, J. N.; Tiwari, R. N.; Chang, Y.-M.; Lin, K.-L. *ChemSusChem* **2010**, *3*, 460–466.
(9) Centi, G.; Perathoner, S. *Eur. J. Inorg. Chem.* **2009**, *26*, 3851–3878.
(10) Sogaard, M.; Odgaard, M.; Skou, E. M. *Solid State Ionics* **2001**, *145*, 31–35.
(11) Lee, E. P.; Peng, Z.; Cate, D. M.; Yang, H.; Campbell, C. T.; Xia, Y. *J. Am. Chem. Soc.* **2007**, *129*, 10634–10635.
(12) Lin, Z.-H.; Lin, M.-H.; Chang, H.-T. *Chem.—Eur. J.* **2009**, *15*, 4656–4662.
(13) Tong, X.; Zhao, G.; Liu, M.; Cao, T.; Liu, L.; Li, P. *J. Phys. Chem. C* **2009**, *113*, 13787–13792.
(14) Ma, Y.; Jiang, S.; Jian, G.; Tao, H.; Yu, L.; Wang, X.; Wang, X.; Zhu, J.; Hu, Z.; Chen, Y. *Energy Environ. Sci.* **2009**, *2*, 224–229.
(15) Kuo, J. W.; Zhao, T. S.; Prabhuram, J.; Chen, R.; Wong, C. W. *Electrochim. Acta* **2005**, *51*, 754–763.
(16) Su, F.; Zhao, X. S.; Wang, Y.; Zeng, J.; Zhou, Z.; Lee, J. Y. *J. Phys. Chem. B* **2005**, *109*, 20200–20206.
(17) Su, F.; Zeng, J.; Bao, X.; Yu, Y.; Lee, J.-Y.; Zhao, X. S. *Chem. Mater.* **2005**, *17*, 3960–3967.
(18) Kabbabi, A.; Faure, R.; Durand, R.; Beden, B.; Hahn, F.; Leger, J. M.; Lamy, C. *J. Electroanal. Chem.* **1998**, *444*, 41–53.
(19) Liu, B.; Chen, J. H.; Zhong, X. X.; Cui, K. Z.; Zhou, H. H.; Kuang, Y. F. *J. Colloid Interface Sci.* **2007**, *307*, 139–144.
(20) Xiao, Z.; Yan, G.; Feng, C.; C H Chan, P.; Hsing, I.-M. *J. Micromech. Microeng.* **2006**, *16*, 2014–2020.

AM100256G